bioRxiv preprint doi: https://doi.org/10.1101/717983; this version posted July 29, 2019. The copyright holder for this preprint (which was not certified by peer review) is the author/funder, who has granted bioRxiv a license to display the preprint in perpetuity. It is made available under aCC-BY-NC-ND 4.0 International license.

Nicotianamine synthase 2 is required for symbiotic nitrogen fixation in *Medicago truncatula* nodules

Viviana Escudero[1], Isidro Abreu[1], Eric del Sastre[1], Manuel Tejada-Jiménez[1], Camile Larue[2], Lorena Novoa-Aponte[3], Jiangqi Wen[4], Kirankumar S. Mysore[4], Javier Abadía[5], José M. Argüello[3], Hiram Castillo-Michel[6], Ana Álvarez-Fernández[5], Juan Imperial[7], Manuel González-Guerrero[1,8*].

[1] Centro de Biotecnología y Genómica de Plantas (UPM-INIA), Universidad Politécnica de Madrid, 28223 Pozuelo de Alarcón (Madrid), Spain.

[2] EcoLab, Université de Toulouse, CNRS, Toulouse, France

[3] Worcester Polytechnic Institute. Worcester MA01609, USA.

[4] Noble Research Institute, Ardmore, OK73401, USA.

[5] Estación Experimental de Aula Dei, Consejo Superior de Investigaciones Científicas, 50059 Zaragoza, Spain.

[6] ID21 Beamline. European Synchrotron Radiation Facility, Grenoble 38043, France.

[7] Instituto de Ciencias Agrarias, Consejo Superior de Investigaciones Científicas, 28006 Madrid, Spain.

[8] Escuela Técnica Superior de Ingeniería Agronómica, Alimentaria y de Biosistemas, Universidad Politécnica de Madrid, 28040 Madrid, Spain.

[*] Corresponding author: manuel.gonzalez@upm.es

Running Head: Medicago NAS2 in symbiotic nitrogen fixation

Keywords: iron, metal homeostasis, legume, NAS

bioRxiv preprint doi: https://doi.org/10.1101/717983; this version posted July 29, 2019. The copyright holder for this preprint (which was not certified by peer review) is the author/funder, who has granted bioRxiv a license to display the preprint in perpetuity. It is made available under aCC-BY-NC-ND 4.0 International license.

SUMMARY

Symbiotic nitrogen fixation carried out by the interaction between legumes and diazotrophic bacteria known as rhizobia requires of relatively large levels of transition metals. These elements act as cofactors of many key enzymes involved in this process. Metallic micronutrients are obtained from soil by the roots and directed to sink organs by the vasculature, in a process participated by a number of metal transporters and small organic molecules that mediate metal delivery in the plant fluids. Among the later, nicotianamine is one of the most important. Synthesized by nicotianamine synthases (NAS), this non-proteinogenic amino acid forms metal complexes participating in intracellular metal homeostasis and long-distance metal trafficking. Here we characterized the *NAS2* gene from model legume *Medicago truncatula*. MtNAS2 is located in the root vasculature and in all nodule tissues in the infection and fixation zones. Symbiotic nitrogen fixation requires of *MtNAS2* function, as indicated by the loss of nitrogenase activity in the insertional mutant *nas2-1*, a phenotype reverted by reintroduction of a wild-type copy of *MtNAS2*. This would be the result of the altered iron distribution in *nas2-1* nodules, as indicated by X-ray fluorescence studies. Moreover, iron speciation is also affected in these nodules. These data suggest a role of nicotianamine in iron delivery for symbiotic nitrogen fixation.

Significance Statement: Nicotianamine synthesis mediated by MtNAS2 is important for iron allocation for symbiotic nitrogen fixation by rhizobia in *Medicago truncatula* root nodules.

bioRxiv preprint doi: https://doi.org/10.1101/717983; this version posted July 29, 2019. The copyright holder for this preprint (which was not certified by peer review) is the author/funder, who has granted bioRxiv a license to display the preprint in perpetuity. It is made available under aCC-BY-NC-ND 4.0 International license.

INTRODUCTION

Nitrogen is one of the main limiting nutrients in the biosphere, in spite of N_2 abundance (Smil, 1999, Hoffman *et al.*, 2014). Nitrogenase is the only enzyme that can convert, fix, N_2 into NH_3 under physiological conditions, in an energy consuming process (Burk, 1934, Burgess and Lowe, 1996). This enzyme is only expressed by the small group of diazotrophic archaea and bacteria, some of them participating in symbiosis with other organisms (Boyd and Peters, 2013). Arguably, one of the best characterized symbiosis with diazotrophic bacteria is the one established between rhizobia and legumes (Brewin, 1991, Downie, 2014). This symbiosis is the basis for legume use in crop rotation strategies and their potential as an alternative to polluting and expensive synthetic nitrogen fertilizers (Johnson and Mohler, 2009, Mus *et al.*, 2016).

Symbiotic nitrogen fixation by the legume-rhizobia system is carried out in root nodules (Downie, 2014). These are differentiated organs that develop after a complex exchange of chemical signals between the symbionts (Oldroyd, 2013). Detection of the nodulation factors released by the rhizobia, triggers cell proliferation in the pericyle-inner cortex of the root to originate nodule primordia (Xiao *et al.*, 2014). As nodules grow, rhizobia from the root surface are directed by infection threads to the nodule cells (Gage, 2002). There, they are released in an endocytic-like process, originating pseudo-organelles known as symbiosomes (Roth and Stacey, 1989, Catalano *et al.*, 2006). Within the symbiosomes, rhizobia differentiate into bacteroids and express the enzymatic machinery required for nitrogen fixation (Kondorosi *et al.*, 2013). Nodule development follows either an indeterminate or a determinate growth pattern, based on whether they maintain an apical meristem to sustain growth (Vasse *et al.*, 1990). As this meristem allows for sustained growth in indeterminate nodules, four developmental zones appear: the meristematic region or Zone I; the infection-differentiation zone or Zone II, where rhizobia are released in the cell and start differentiating; the fixation zone or Zone III, where nitrogenase is active; and the senescent zone or Zone IV, where symbiosomes are degraded and nutrients recycled (Burton *et al.*, 1998). In addition, some authors define a transition interzone between Zones II and III (Roux *et al.*, 2014).

Nutrient exchange between the symbionts enables nitrogen fixation (Udvardi and Poole, 2013). Availability of fixed nitrogen forms in soils inhibits nodulation (Streeter, 1987). Similarly, low levels of photosynthates, phosphate or sulphate transfer from the host plant decrease nodulation and nitrogen fixation rates (Singleton and van Kessel,

bioRxiv preprint doi: https://doi.org/10.1101/717983; this version posted July 29, 2019. The copyright holder for this preprint (which was not certified by peer review) is the author/funder, who has granted bioRxiv a license to display the preprint in perpetuity. It is made available under aCC-BY-NC-ND 4.0 International license.

1987, Valentine *et al.*, 2017, Schneider *et al.*, 2019). Transition metals such as iron, copper, zinc, or molybdenum are also critical for nodulation and nitrogen fixation as cofactors in many of the involved enzymes (González-Guerrero *et al.*, 2014, González-Guerrero *et al.*, 2016). This includes not only nitrogenase (Rubio and Ludden, 2005), but also NADPH-oxidases that participate in nodule signalling (Montiel *et al.*, 2016), leghemoglobin that maintains nodule O_2 homeostasis (Appleby, 1984), high-affinity cytochrome oxidases providing energy to the bacteroids (Preisig *et al.*, 1996), as well as many enzymes involved in free radical control (Dalton *et al.*, 1998, Santos *et al.*, 2000, Rubio *et al.*, 2007). Consequently, deficiencies in the uptake of these nutrients or alterations in the metal delivery pathways lead to defects in nodulation and/or nitrogen fixation (Tang *et al.*, 1991, O'Hara, 2001, Senovilla *et al.*, 2018, Gil-Díez *et al.*, 2019).

To reach the bacteroids, metals must first cross from soil into the roots using the general mechanisms common to all dicots (Kobayashi and Nishizawa, 2012, Curie and Mari, 2017). Metal uptake is facilitated by soil acidification, the release of phenolics/coumarins and flavins, and cation reduction when required (Jain *et al.*, 2014). Metals are then introduced into the root epidermis and symplastically or apoplastically reach the root endodermis, to cross into the vasculature, and delivered to sink organs. In model legume *Medicago truncatula* metals are released from the vessels into the apoplast of the infection-differentiation zone of nodules (Rodríguez-Haas *et al.*, 2013). These nutrients will be introduced in rhizobia-infected cells and targeted to symbiosomes for nitrogen fixation. In recent years, many of the membrane transporters participating in metal transfer from the plant to the bacteroids have been identified. For instance, iron transfer to nitrogen-fixing cells is facilitated by plasma membrane iron uptake protein MtNramp1 (Tejada-Jiménez *et al.*, 2015), and its transport across the symbiosome membrane by MtSEN1 and MtFPN2 (Hakoyama *et al.*, 2012, Escudero *et al.*, 2019). However, little is known on how metals are sorted intracellularly and on the speciation of these elements.

Unlike alkali or alkali-earth elements, transition metals are not “free”, hydrated, in physiological solutions. Instead, they are bound to a plethora of organic molecules that maintain them soluble under different pH, prevent metal-catalysed production of free radicals in Fenton-style reactions, and avoid mis-metallation of enzymes (Finney and Halloran, 2003, Rellán-Álvarez *et al.*, 2008, Flis *et al.*, 2016). Systematic studies of the nature of these chemical species in the sap of model plants have revealed the importance

bioRxiv preprint doi: https://doi.org/10.1101/717983; this version posted July 29, 2019. The copyright holder for this preprint (which was not certified by peer review) is the author/funder, who has granted bioRxiv a license to display the preprint in perpetuity. It is made available under aCC-BY-NC-ND 4.0 International license.

of citrate and nicotianamine in this role (von Wiren *et al.*, 1999, Durrett *et al.*, 2007, Roschzttardtz *et al.*, 2011, Schuler *et al.*, 2012). Citrate is the main iron chelator in xylem and facilitates iron delivery across symplastically disconnected tissues (Durrett *et al.*, 2007, Rellán-Álvarez *et al.*, 2010, Roschzttardtz *et al.*, 2011). It has also been associated with iron trafficking to nodules (LeVier *et al.*, 1996). Citrate efflux proteins LjMATE1 and MtMATE67 are required for iron allocation to nodules and contribute to nitrogen fixation (Takanashi *et al.*, 2013, Kryvoruchko *et al.*, 2018). Citrate efflux is also important for iron delivery to bacteroids, as indicated by the symbiosome localization of nodule-specific protein MtMATE67 (Kryvoruchko *et al.*, 2018).

Nicotianamine is also an important player in plant metal homeostasis. This molecule is a non-proteinogenic amino acid synthesized by nicotianamine synthases (NAS) from S-adenosyl methionine (Higuchi *et al.*, 1999). Nicotianamine-metal complexes mediate long-distance metal trafficking, particularly along the phloem, as well as participate in vacuolar metal storage (von Wiren *et al.*, 1999, Haydon *et al.*, 2012, Flis *et al.*, 2016). A nodule-specific NAS gene was identified in senescent nodules of *L. japonicus*, likely participating in the metal redistribution to the developing flowers and embryos, as orthologues do with older leaves (Hakoyama *et al.*, 2009, Schuler *et al.*, 2012). No such nodule-specific NAS gene can be found in transcriptomic databases from indeterminate type nodules, but tentative evidence shows that a *M. truncatula* NAS protein, MtNAS1, might be responsible for iron allocation to these organs (Avenhaus *et al.*, 2016). Here, we have characterized a second NAS protein, MtNAS2, identified in a screening of *M. truncatula Tnt1*-insertion mutants. This gene, although primarily expressed in roots, is important for metal allocation for symbiotic nitrogen fixation.

RESULTS

Medicago truncatula Tnt1 line NF15101 phenotype is due to transposon insertion in *MtNAS2*

A search for metal-related symbiotic phenotypes of the mutants available at the Noble Research Institute *M. truncatula* Mutant Database showed NF15101 as one of the available mutants with a nitrogen fixation deficient phenotype. This line has 22 *Tnt1* insertions, 10 of which interrupted different *M. truncatula* genes (Supp. Table 1), *Medtr2g070310* among them. This gene encodes a protein with 52 % identity and 67 %

bioRxiv preprint doi: https://doi.org/10.1101/717983; this version posted July 29, 2019. The copyright holder for this preprint (which was not certified by peer review) is the author/funder, who has granted bioRxiv a license to display the preprint in perpetuity. It is made available under aCC-BY-NC-ND 4.0 International license.

similarity to *Arabidopsis thaliana* NAS2 protein, and consequently was renamed *MtNAS2*. *MtNAS2* was expressed at similar levels in roots from plants inoculated or non-inoculated with *Sinorhizobium meliloti* (Fig. 1A). Significantly, lower expression was detected in nodules, and no signal was detected in shoots from either inoculated or non-inoculated plants. *Tnt1* was inserted in position +760 of *MtNAS2*, interrupting the reading frame of its only exon and diminishing *MtNAS2* mRNA levels below our detection limit (Fig. 1B). As expected, NF15101, *nas2-1* in this report, had reduced biomass production in nitrogen fixation conditions (Fig. 2A, B). While nodule development and nodule number were not significantly altered in *nas2-1* compared to wild type (Fig. 2C, D, Supp. Fig. 1), nitrogenase activity was reduced three-fold in *nas2-1* plants (Fig. 2E). No significant differences in nicotianamine content were observed between wild-type and mutant plants (Supp. Fig. 2). The *nas2-1* phenotype was reverted when a wild-type copy of *MtNAS2* regulated by its own promoter was reintroduced in *nas2-1* (Fig. 2). The data indicate that among all the *Tnt1* insertions, loss of *MtNAS2* function was determinant for the reduction of nitrogenase activity and overall growth alterations.

***MtNAS2* is not required for plant growth under non-symbiotic conditions**

To determine whether the symbiotic phenotype of *nas2-1* was the result of additional physiological processes being affected, these plants and their controls were grown in the same conditions as above, but supplemented with ammonium nitrate in the nutrient solution to compensate for the lack of rhizobial inoculation. In these conditions, no significant differences were found in plant growth, biomass production, or chlorophyll content between wild-type and *nas2-1* plants (Fig. 3). Considering the role of nicotianamine in plant iron homeostasis (von Wiren *et al.*, 1999, Inoue *et al.*, 2003) and the added pressure of symbiotic nitrogen fixation on iron nutrition (Terry *et al.*, 1991), *nas2-1* phenotype was also studied under non-symbiotic, low-iron conditions (no iron added to the nutrient solution). Low-iron supply did not lead to different growth between control and *nas2-1* plants (Supp. Fig. 3).

***MtNAS2* is expressed in the xylem parenchyma in roots and in the nodule fixation zone**

bioRxiv preprint doi: https://doi.org/10.1101/717983; this version posted July 29, 2019. The copyright holder for this preprint (which was not certified by peer review) is the author/funder, who has granted bioRxiv a license to display the preprint in perpetuity. It is made available under aCC-BY-NC-ND 4.0 International license.

188 The physiological role of *MtNAS2* is determined by its differential tissue and
189 cellular expression. To establish the gene tissue expression, *M. truncatula* plants were
190 transformed with a binary vector containing the *MtNAS2* promoter region driving the *β-*
191 *glucuronidase* (*gus*) gene transcription and GUS activity visualized using X-Gluc.
192 *MtNAS2* was expressed in roots and nodules (Fig. 4A), in agreement with the transcript
193 data (Fig. 1). Longitudinal section of the nodules showed GUS activity in cells in the
194 interzone and fixation zone of the nodule (Fig. 4B). Nodule cross-sections showed
195 expression in all nodule tissues (Fig. 4C). In roots, *MtNAS2* promoter was active in
196 vasculature cells (Fig. 4D).

197 Supporting the gene expression results, immunolocalization of HA-tagged
198 MtNAS2 under control of its own promoter showed that the protein was located in cells
199 neighbouring the interzone and fixation zone (Fig. 5A). At higher magnification, we
200 could observe that MtNAS2-HA had a homogenous distribution within the cells, and it
201 did not seem to cluster in any particular location (Fig. 5B). Analysis of nodule vasculature
202 showed MtNAS2-HA in endodermal cells (Fig. 5C). However, in the root vasculature,
203 MtNAS2-HA was detected in small cells associated to the xylem, (Fig. 5D). Controls
204 were carried out to ensure that the data did not stem from autofluorescence (Supp. Fig 4).

205

206 **_MtNAS2_ is required for efficient metal allocation for symbiotic nitrogen fixation**

207 Nicotianamine is required for metal allocation from source to sink tissues (Schuler
208 *et al.*, 2012). Alterations in nicotianamine synthesis typically lead to reduced metal
209 delivery to sink tissues. To determine whether this was the case for *nas2-1*, iron, copper
210 and zinc levels in roots, shoots, and nodules from 28 days-post-inoculation (dpi) plants
211 were determined. No significant changes in these levels were observed (Fig. 6A).
212 However, metal allocation might be altered while not affecting total nodule metal content.
213 To assess this possibility, synchrotron-based X-ray fluorescence studies were carried out
214 to determine iron distribution in *nas2-1* compared to wild type (Fig. 6B). These
215 experiments showed that iron distribution was altered in *nas2-1* mutants. To further
216 confirm that mutation of *MtNAS2* affected iron distribution in nodules as a consequence
217 of changes of iron speciation, X-ray Absorption Near-Edge Spectroscopy (XANES)
218 analyses of iron speciation in the different nodule developmental zones were carried out
219 (Fig. 6C). Principal component analyses of these spectra showed that the iron complexes

bioRxiv preprint doi: https://doi.org/10.1101/717983; this version posted July 29, 2019. The copyright holder for this preprint (which was not certified by peer review) is the author/funder, who has granted bioRxiv a license to display the preprint in perpetuity. It is made available under aCC-BY-NC-ND 4.0 International license.

in the fixation zone were quite different (Fig. 6D). Fitting of the obtained spectra to known standards showed that the proportion of Fe-S complexes had a dramatic drop in *nas2-1* compared to wild-type plants, while the proportion of O/N complexes with iron had a larger increase (Table 1).

DISCUSSION

Metallic micronutrient delivery to nodules is essential for symbiotic nitrogen fixation, as they are cofactors in many of the involved enzymes (Brear *et al.*, 2013, González-Guerrero *et al.*, 2014). In recent years, studies have shown how metals are exported to the apoplast in the infection/differentiation zone of *M. truncatula* nodules (Rodríguez-Haas *et al.*, 2013), and transmembrane transporters introduce metals into rhizobia-infected cells (Tejada-Jiménez *et al.*, 2015, Abreu *et al.*, 2017, Tejada-Jiménez *et al.*, 2017, Senovilla *et al.*, 2018), or deliver iron to the bacteroids (Escudero et al., 2019). In this transport, citrate participates in maintaining iron solubility in the apoplast, and as the preferred iron source for bacteroids (Moreau *et al.*, 1995, LeVier *et al.*, 1996, Kryvoruchko *et al.*, 2018). Here we show that nicotianamine synthesis is also important for correct iron allocation to *M. truncatula* nodules.

Interrupting *MtNAS2* expression with a transposon insertion led to reduced plant growth in symbiotic conditions, a consequence of lower nitrogenase activity. Although several genes were affected in the studied *Tnt1* line, reintroduction of a wild-type copy of *MtNAS2* was sufficient to restore wild-type growth. Consequently, the mutation of this gene was mainly responsible for the observed phenotype. While important under symbiotic conditions, *MtNAS2* seemed to be playing a secondary role when plants were not inoculated but watered with an ammonium nitrate-supplemented nutrient solution instead. This is in contrast to the substantially higher expression levels of *MtNAS2* in roots than in nodules. This observation would suggest a predominant role in nicotianamine synthesis in roots. However, studies in *A. thaliana* reveal the existence of a high redundancy rate in the NAS family, where a quadruple *nas* mutant was required to observe a substantial phenotype, including limited growth (Klatte *et al.*, 2009). Similarly, no significant changes in nicotianamine content were observed in single *nas A. thaliana* lines, as neither was observed in *M. truncatula nas2-1*. Two possible causes might explain the symbiosis-specific phenotype of *nas2-1* plants. One of them is that MtNAS2 would be required to compensate for the enhanced iron requirements of nodulated plants. This

bioRxiv preprint doi: https://doi.org/10.1101/717983; this version posted July 29, 2019. The copyright holder for this preprint (which was not certified by peer review) is the author/funder, who has granted bioRxiv a license to display the preprint in perpetuity. It is made available under aCC-BY-NC-ND 4.0 International license.

253 additional nutritional pressure would trigger the observed *nas2-1* phenotype. If so, we
254 should have also observed a similar phenotype when plants were watered with an iron-
255 restricted nutrient solution, which has been shown in the past to elicit the iron deficiency
256 response in *M. truncatula* (Andaluz *et al.*, 2009, Tejada-Jiménez *et al.*, 2015). However,
257 this was not observed. Alternatively, in a more parsimonious mechanism,
258 neofunctionalization of pre-existing genes during the development of symbiotic nitrogen
259 fixation might have led to the loss of functional redundancy. Similar observations have
260 been made when studying other *M. truncatula* metal homeostasis genes that, although
261 expressed in roots and in nodules, exhibit phenotypes limited to nodulation and nitrogen
262 fixation (Tejada-Jiménez *et al.*, 2015, Abreu *et al.*, 2017, León-Mediavilla *et al.*, 2018).

263 In roots, *MtNAS2* was expressed at high levels in xylem parenchyma cells,
264 similarly to rice *NAS2* (Inoue *et al.*, 2003). Vascular localization of NAS proteins is not
265 unusual, since they have been associated to long distance metal trafficking (von Wiren *et*
266 *al.*, 1999, Kumar *et al.*, 2017). This vascular localization of MtNAS2 was also observed
267 in nodules. However, the cellular localization of the protein is different to what was
268 observed in roots; in nodules, most of vascular MtNAS2 was confined to the endodermis.
269 This alternative distribution of MtNAS2 in vessels could be indicative of differential
270 functions. Root vascular localization could indicate a role in metal loading of the vascular
271 fluids, while endodermal localization in nodules might mediate either uptake from saps
272 or intracellular metal trafficking. In any case, it seems unlikely that the nicotianamine
273 synthesized by nodule endodermal cells would end up in the apoplast, since citrate-iron
274 complexes seem to be formed in this compartment at a pH that does not facilitate iron-
275 nicotianamine association (Rellán-Álvarez *et al.*, 2008).

276 *MtNAS2* expression in nodule core cells in the interzone and zone III also indicates
277 a role of nicotianamine in metal homeostasis of nitrogen fixing cells. It has been
278 previously described that nicotianamine can participate in intracellular metal trafficking
279 and in cell-to-cell metal delivery, as well as serve as intracellular storage of metals
280 (Haydon *et al.*, 2012). Mutation of *MtNAS2* did not significantly alter iron, copper, or
281 zinc levels in any of the plant organs analysed, but a major shift in iron distribution was
282 observed in nodules, with a significant decrease of iron accumulation in the interzone and
283 early fixation zone. This would indicate that iron trafficking in these cells is altered.
284 However, MtNAS2-mediated iron trafficking would only affect a subset of the nodule
285 iron-proteome, since delivery to the fixation zone was not completely blocked as attested

bioRxiv preprint doi: https://doi.org/10.1101/717983; this version posted July 29, 2019. The copyright holder for this preprint (which was not certified by peer review) is the author/funder, who has granted bioRxiv a license to display the preprint in perpetuity. It is made available under aCC-BY-NC-ND 4.0 International license.

by the red colour of nodules, indicative that leghemoglobin (an important iron sink) was being produced in addition to a residual nitrogenase activity. This could suggest the existence of differential metallation pathways in nodules that might serve different subsets of proteins, which could partially complement each other under stress conditions. Supporting this hypothesis, mutation of *MtNAS2* did not equally affect all the iron species in the fixation zone. While the percentage of iron-sulfur complexes detected by XANES was significantly lower than in control plants, iron coordinated by nitrogen or oxygen atoms was increased. Considering the high demand for iron-sulfur clusters for nitrogenase assembly (Rubio and Ludden, 2005), its decrease could explain the reduction of nitrogenase activity observed. The changes in iron speciation were particularly severe in the fixation zone, which is consistent with *MtNAS2* distribution, with the observed reduction of nitrogenase activity, and with the iron distribution data. It is important to indicate that we cannot rule out similar effects on copper or zinc speciation and distribution, since the synchrotron setup available to us at the European Synchrotron Radiation Facility prevented us to carry out similar analyses on those two elements.

This work highlights the importance of MtNAS2 in iron delivery for symbiotic nitrogen fixation. This is not the only NAS gene that might be involved in the process, since total nicotianamine production is sustained in nodules, and other family members have been shown to be expressed in these organs, such as MtNAS1 (Avenhaus *et al.*, 2016). The localization of MtNAS2 indicates that nicotianamine would be involved in intracellular iron trafficking that is highly important for nitrogenase functioning. This role would not be directly providing the element to the bacteroid, since iron-citrate seems to be the key here, but perhaps would shuttle this element in the cytosol. However, to better define this possibility, new tools in elemental imaging and speciation with higher resolution within a cell need to be established to track iron and other elements. In addition, the roles of ZIF-like (Haydon *et al.*, 2012)and YSL proteins (Waters *et al.*, 2006) in symbiotic nitrogen fixation must be determined. Finally, other NAS proteins might facilitate iron recycling in *M. truncatula* nodules, as it occurs in *L. japonicus* (Hakoyama *et al.*, 2009).

EXPERIMENTAL PROCEDURES

Biological material and growth conditions

bioRxiv preprint doi: https://doi.org/10.1101/717983; this version posted July 29, 2019. The copyright holder for this preprint (which was not certified by peer review) is the author/funder, who has granted bioRxiv a license to display the preprint in perpetuity. It is made available under aCC-BY-NC-ND 4.0 International license.

M. truncatula Gaertn R108 and *nas2-1* (NF15101) seeds were scarified in concentrated sulfuric acid (96%) for 7.5 min. After removing the acid, the seeds were washed eight times with cold water, and surface-sterilized with 50 % (v/v) bleach for 90 s. Seeds were embedded overnight in the dark at room temperature in sterile water, and transferred to 0.8 % water-agar plates for 48 h at 4 ºC (stratification). Germination was carried out at 22 ºC in the dark. Seedlings were planted on sterile perlite pots, and inoculated with *S. meliloti* 2011 or the same bacterial strain transformed with pHC60 (Cheng and Walker, 1998). Plants were grown in a greenhouse under 16 h light / 8 h dark at 25 ºC / 20 ºC conditions. In the case of perlite pots, plants were watered every two days with Jenner's solution or water alternatively (Brito *et al.*, 1994). Nodules were obtained at 28 dpi. Plants growing in non-symbiotic conditions were watered every two weeks with a nutrient solution supplemented with 20 mM NH_4NO_3. For hairy-root transformation experiments, *M. truncatula* seedlings were transformed with *Agrobacterium rhizogenes* strain ARqua1, fused to the appropriate binary vector as described (Boisson-Dernier *et al.*, 2001).

RNA Extraction and Quantitative real-time RT-qPCR

RNA was extracted from 28 dpi plants using TRI-reagent (Life Technologies), treated using DNase turbo (Life Technologies), and cleaned with RNeasy Mini-kit (Qiagen). cDNA was obtained from 500 ng RNA using PrimeScript RT reagent Kit (Takara). Expression studies were carried out by real-time reverse transcription polymerase chain reaction (RT-qPCR; StepOne plus, Applied Biosystems) using the Power SyBR Green master mix (Applied Biosystems). The primers used are indicated in Supp. Table 2. RNA levels were normalized by using the ubiquitin conjugating enzyme E2 (*Medtr7g116940*) gene as internal standard. Real time cycler conditions have been previously described (González-Guerrero *et al.*, 2010).

GUS Staining

MtNAS2 promoter region was obtained by amplifying the 1940 bp upstream of the start codon using the primers indicated in Supp.Table 2, and cloned by Gateway cloning technology (Invitrogen) in pDONR207 (Invitrogen) and transferred to destination vector pGWB3 (Nakagawa *et al.*, 2007). Hairy-root transformations of *M. truncatula* seedlings were carried out with *A. rhizogenes* ARqua1 as described by Boisson-Denier *et al*. (2001). After three weeks on Fahreus media plates with kanamycin (50 µg/mL), plant

bioRxiv preprint doi: https://doi.org/10.1101/717983; this version posted July 29, 2019. The copyright holder for this preprint (which was not certified by peer review) is the author/funder, who has granted bioRxiv a license to display the preprint in perpetuity. It is made available under aCC-BY-NC-ND 4.0 International license.

transformants were transferred to sterilized perlite pots and inoculated with *S. meliloti* 2011. GUS activity was determined in 28 dpi plants as described (Vernoud *et al.*, 1999).

Confocal microscopy

The coding sequence region of *MtNAS2* and 1940 bp upstream of its start codon were cloned in pGWB13 vector (Nakagawa et al., 2007) using Gateway cloning technology (Invitrogen). This fuses three HA epitopes to C-terminus of the protein. Hairy-root *M. truncatula* transformants were transferred to sterilized perlite pots and inoculated with *S. meliloti* 2011 containing the pHC60 plasmid that constitutively expresses GFP. Nodules and roots were collected from 28 dpi plants and fixed at 4 ºC overnight in 4 % para-formaldehyde and 2.5 % sucrose in phosphate-buffered saline (PBS). Fixative was removed by washing for 5 min in PBS and 5 min in water. Nodule and roots were included in 6 % agarose for sectioning with a Vibratome 1000 Plus. Sections were dehydrated by serial incubation with methanol (30 %, 50 %, 70 % and 100 % in PBS) for 5 min and then rehydrated following the same methanol series in reverse order. Cell wall permeabilization was carried out by incubation with 2 % (w/v) cellulase in PBS for 1 h and 0.1 % (v/v) Tween 20 for 15 min. Sections were blocked with 5% (w/v) bovine serum albumin in PBS and then incubated with 1:50 anti-HA mouse monoclonal antibody (Sigma) in PBS at room temperature for 2 h. Primary antibody was washed three times with PBS for 15 min and subsequently incubated with 1:40 Alexa 594-conjugated anti-mouse rabbit monoclonal antibody (Sigma) in PBS at room temperature for 1 h. Secondary antibody was washed three times with PBS for 10 min. DNA was stained using DAPI. Images were obtained with a confocal laser-scanning microscope (Leica SP8) using excitation light at 488 nm to GFP and 561 nm for Alexa 594.

Acetylene reduction assays

Nitrogenase activity assay was measured by acetylene reduction test (Hardy *et al.*, 1968). Wild-type and *nas2-1* nodulated roots from 28 dpi were separately introduced in 30 ml vials. Each tube contained four or five independently transformed plants. Three milliliters of air from each bottle was replaced by the same volume of acetylene, tubes were subsequently incubated for 30 min at room temperature. Gas samples were measured by analyzing 0.5 ml of ethylene from each bottle in a Shimadzu GC-8A gas chromatograph using a Porapak N column. The amount of the ethylene produced was determined by measuring the ethylene peaks relative to the standards.

bioRxiv preprint doi: https://doi.org/10.1101/717983; this version posted July 29, 2019. The copyright holder for this preprint (which was not certified by peer review) is the author/funder, who has granted bioRxiv a license to display the preprint in perpetuity. It is made available under aCC-BY-NC-ND 4.0 International license.

386

387 Chlorophyll Content Assays

388 Total chlorophyll content was determined as previously described with some
389 modifications (Inskeep and Bloom, 1985). Leaves were collected from 28 dpi plants and
390 poled to obtain 50 mg of fresh material. Chlorophyll was extracted with 500 µl of di-
391 methyl-formamide at 4 ºC overnight. Leaves were centrifuged for 5 min at 600 g at room
392 temperature. After transferring the supernatant to another vial, the chlorophyll extraction
393 was repeated with the same leave using strong vortexing. After spinning for 5 min at 600
394 g, the supernatant was pooled with the previous one. Chlorophyll was quantified at 647
395 nm and 664 nm in a Ultraspec 3300 spectrophotometer (Amershan Bioscience).

396

397 Metal content determination

398 Shoots, roots, and nodules were collected from 28 dpi plants and mineralized with
399 15.6 M HNO_3 (trace metal grade) at 75°C for 3 h and 2 M H_2O_2 at 20°C overnight. Metal
400 quantifications were performed in duplicate by Atomic Absorption Spectroscopy, using
401 a Perkin Elmer PinAAcle 900Z GF-AAS equipment. Metal concentration was normalized
402 against fresh tissue weight.

403

404 Synchrotron Radiation X-Ray Fluorescence Spectroscopy (XRF) and XANES

405 XRF hyperspectral images and µXANES spectra were acquired on the beamline
406 ID21 of the European Synchrotron Radiation Facility (Cotte *et al.*, 2017), at 110 K in the
407 liquid nitrogen (LN2) cooled cryostat of the Scanning X-ray Micro-spectroscopy end-
408 station. Seven sections from *M. truncatula* R108 nodules and five from *nas2-1* nodules
409 were obtained from different nodules embedded in OCT medium and cryo-fixed by
410 plunging in isopentane chilled with LN2. The 25 µm-thick sections of frozen samples
411 were obtained using a Leica LN2 cryo-microtome and accommodated in a Cu sample
412 holder cooled with LN2, sandwiched between Ultralene (SPEX SamplePrep) foils. The
413 beam was focused to 0.4×0.9 μm^2 with a Kirkpatrick-Baez (KB) mirror system. The
414 emitted fluorescence signal was detected with energy-dispersive, large area (80 mm^2)
415 SDD detector equipped with Be window (SGX from RaySpec). Images were acquired at
416 the fixed energy of 7.2 keV, by raster-scanning the sample in the X-ray focal plane, with
417 a step of 3×3 μm^2 and 100 ms dwell time. Elemental mass fractions were calculated from
418 fundamental parameters with the PyMCA software package, applying pixel-by-pixel
419 spectral deconvolution to hyperspectral maps normalized by the incoming flux (Solé *et*

bioRxiv preprint doi: https://doi.org/10.1101/717983; this version posted July 29, 2019. The copyright holder for this preprint (which was not certified by peer review) is the author/funder, who has granted bioRxiv a license to display the preprint in perpetuity. It is made available under aCC-BY-NC-ND 4.0 International license.

al., 2007). The incoming flux was monitored using a drilled photodiode previously calibrated by varying the photon flux at 7.2 keV obtaining a response of 1927.9 charges/photon with a linear response up to 200 kcps. In PyMCA the incoming flux and XRF detector parameters were set to $2x10^9$ photons/s, 0.7746 cm^2 active area, and 4.65 cm sample to XRF detector distance. Sample matrix was assumed to be amorphous ice (11% H, 89% O, density 0.92 g/cm^3), the sample thickness set at 25µm obtained with the use of a cryo-microtome.

Fe-K edge (7.050 to 7.165 keV energy range, 0.5 eV step) µXANES spectra were recorded in regions of interest of the fluorescence maps acquired on ID21 beamline. Individual spectra were processed using Orange software with the Spectroscopy add-on (Demsar *et al.*, 2013). The pre-processing step consisted of vector normalization and a Savitsky-Golay filter for the smoothing. Then a principal component analysis was performed on the second derivative of the spectra to highlight potential differences among genotypes within a given region of the nodule. A reference library was used for linear combination fitting (LCF) procedure. This library consisted of: Fe-foil (Fe(0)), Fe(II)-nicotianamine, Fe(II)S2 (http://ixs.iit.edu/database/), Fe(III)-haem (50 mM, pH7, bought from Sigma, CAS number: 16009-13-5), Fe(III)-cellulose (5 mM $FeCl_3$ + 50 mM cellulose, pH 5.8, bought from Sigma, CAS number: 9004-34-6), Fe(III) glutamic acid (5 mM $FeCl_3$ + 50 mM glutamic acid, pH 7, bought from Sigma, CAS number: 56-86-0) and Fe(III) ferritin (bought from Sigma, CAS number: 9007-73-2, 50 mM, pH7).Reference compounds were classified as Fe(II)-S (FeS2), Fe(II)-O/N (Fe-NA) and Fe(III)-O (Fe-cellulose, Fe-glutamic acid and ferritin). XANES data treatment was performed using Athena software (Ravel and Newville, 2005) as previously described (Larue *et al.*, 2014).

Statistical tests

Data were analyzed by Student's unpaired *t* test to calculate statistical significance of observed differences. Test results with *p*-values < 0.05 were considered as statistically significant.

Acknowledgments

This research was funded by a European Research Council Starting Grant (ERC-2013-StG-335284) and a Ministerio de Economía y Competitividad (MINECO) grant (AGL2015-65866-P), to MGG, and a MINECO grant (AGL2016-75226-R) to JA and

bioRxiv preprint doi: https://doi.org/10.1101/717983; this version posted July 29, 2019. The copyright holder for this preprint (which was not certified by peer review) is the author/funder, who has granted bioRxiv a license to display the preprint in perpetuity. It is made available under aCC-BY-NC-ND 4.0 International license.

AA-F. VE was partially funded by the Severo Ochoa Programme for Centres of Excellence in R&D from Agencia Estatal de Investigación of Spain (grant SEV-2016-0672) to CBGP. IA is recipient of a Juan de la Cierva- Formación postodoctoral fellowship from Ministerio de Ciencia, Innovación y Universidades (FJCI-2017-33222). Development of *M. truncatula Tnt1* mutant population was, in part, funded by the National Science Foundation, USA (DBI-0703285) to KSM. We would like to thank Dr. Marine Cotte and Dr Juan Herrera-Estrella for assistance in using beamline ID21 during experiments EV246 and EV323. We would also like to acknowledge the other members of laboratory 281 at Centro de Biotecnología y Genómica de Plantas (UPM-INIA) for their support and feedback in preparing this manuscript.

bioRxiv preprint doi: https://doi.org/10.1101/717983; this version posted July 29, 2019. The copyright holder for this preprint (which was not certified by peer review) is the author/funder, who has granted bioRxiv a license to display the preprint in perpetuity. It is made available under aCC-BY-NC-ND 4.0 International license.

488 **SHORT LEGEND FOR SUPPORTING INFORMATION**

489 **Supporting Figure 1.** Anatomy of 28 dpi wild-type and *nas2-1* nodules.

490 **Supporting Figure 2.** Nicotianamine content in wild-type and *nas2-1* plants.

491 **Supporting Figure 3**. Phenotype of *nas2-1* plants under low iron conditions.

492 **Supporting Figure 4.** Control for immunolocalization assays.

493 **Supporting Table 1**. Genes affected by *Tnt1* insertion in *M. truncatula* line NF15101.

494 **Supporting Table 2.** Primers used in this study.

495 **Supporting Materials and Methods**

496

497

498

499

500

501

502

503

504

505

506

507

508

509

510

511

512

513

bioRxiv preprint doi: https://doi.org/10.1101/717983; this version posted July 29, 2019. The copyright holder for this preprint (which was not certified by peer review) is the author/funder, who has granted bioRxiv a license to display the preprint in perpetuity. It is made available under aCC-BY-NC-ND 4.0 International license.

REFERENCES

Abreu, I., Saez, A., Castro-Rodríguez, R., Escudero, V., Rodríguez-Haas, B., Senovilla, M., Larue, C., Grolimund, D., Tejada-Jiménez, M., Imperial, J. and Gonzalez-Guerrero, M. (2017) *Medicago truncatula* Zinc-Iron Permease6 provides zinc to rhizobia-infected nodule cells. *Plant Cell Environ.*, **40**, 2706-2719.

Andaluz, S., Rodríguez-Celma, J., Abadía, A., Abadía, J. and López-Millán, A.-F. (2009) Time course induction of several key enzymes in *Medicago truncatula* roots in response to Fe deficiency. *Plant Physiol. Biochem.*, **47**, 1082-1088.

Appleby, C.A. (1984) Leghemoglobin and *Rhizobium* respiration. *Annu. Rev. Plant Physiol.*, **35**, 443-478.

Avenhaus, U., Cabeza, R.A., Liese, R., Lingner, A., Dittert, K., Salinas-Riester, G., Pommerenke, C. and Schulze, J. (2016) Short-term molecular acclimation processes of legume nodules to increased external oxygen concentration. *Front. Plant Sci.*, **6**, 1012.

Boisson-Dernier, A., Chabaud, M., Garcia, F., Bécard, G., Rosenberg, C. and Barker, D.G. (2001) Agrobacterium rhizogenes-transformed roots of *Medicago truncatula* for the study of nitrogen-fixing and endomycorrhizal symbiotic associations. *Mol. Plant Microbe Interact.*, **14**, 695-700.

Boyd, E.S. and Peters, J.W. (2013) New insights into the evolutionary history of biological nitrogen fixation. *Front. Microbiol.*, **4**, 201.

Brear, E.M., Day, D.A. and Smith, P.M.C. (2013) Iron: an essential micronutrient for the legume–rhizobium symbiosis. *Front. Plant Sci.*, **4**, 359.

Brewin, N.J. (1991) Development of the legume root nodule. *Annu Rev. Cell Biol.*, **7**, 191-226.

Brito, B., Palacios, J.M., Hidalgo, E., Imperial, J. and Ruíz-Argüeso, T. (1994) Nickel availability to pea (*Pisum sativum* L.) plants limits hydrogenase activity of *Rhizobium leguminosarum* bv. *viciae* bacteroids by affecting the processing of the hydrogenase structural subunits. *J. Bacteriol.*, **176**, 5297-5303.

Burgess, B. and Lowe, D. (1996) Mechanism of molybdenum nitrogenase. *Chem. Rev.*, **96**, 2983-3011.

Burk, D. (1934) Azotase and nitrogenase in *Azotobacter*. *Enzymforsch*, **3**, 23-56.

Burton, J.W., Harlow, C. and Theil, E.C. (1998) Evidence for reutilization of nodule iron in soybean seed development. *J. Plant Nutr.*, **5**, 913-927.

Catalano, C.M., Czymmek, K.J., Gann, J.G. and Sherrier, D.J. (2006) *Medicago truncatula* syntaxin SYP132 defines the symbiosome membrane and infection droplet membrane in root nodules. *Planta*, **225**, 541-550.

Cheng, H.P. and Walker, G.C. (1998) Succinoglycan is required for initiation and elongation of infection threads during nodulation of alfalfa by *Rhizobium meliloti*. *J. Bacteriol.*, **180**, 5183-5191.

Cotte, M.P.E., Salomé, M., Rivard, C., Nolf, W.D., Castillo-Michel, H., Fabris, T., Monico, L., Janssens, K., Wang, T., Sciau, P., Verger, L., Cormier, L., Dargaud, O., Brun, E., Bugnazet, D., Fayard, B., Hesse, B., del Real, A.E.P., Veronesi, G., Langlois, J., Balcar, N., Vandenberghe, Y., Solé, V.A., Kieffer, J., Barrett, R., Cohen, C., Cornu, C., Baker, R., Gagliardini, E., Papillon, E. and Susini, J. (2017) The ID21 X-ray and infrared microscopy beamline at the ESRF: status and recent applications to artistic materials. *J. Anal. At. Spectrom.*, **32**, 477-493.

bioRxiv preprint doi: https://doi.org/10.1101/717983; this version posted July 29, 2019. The copyright holder for this preprint (which was not certified by peer review) is the author/funder, who has granted bioRxiv a license to display the preprint in perpetuity. It is made available under aCC-BY-NC-ND 4.0 International license.

562 **Curie, C. and Mari, S.** (2017) New routes for plant iron mining. *New Phytol.*, **214**, 521-
563 525.
564 **Dalton, D.A., Joyner, S.L., Becana, M., Iturbe-Ormaetxe, I. and Chatfield, J.M.**
565 (1998) Antioxidant defenses in the peripheral cell layers of legume root nodules.
566 *Plant Physiol.*, **116**, 37-43.
567 **Demsar, J., Curk, T., Erjavec, A., Gorup, C., Hocevar, T., Milutinovic, M., Mozina,**
568 **M., Polajnar, M., Toplak, M., Staric, A., Stajdohar, M., Umek, L., Zagar, L.,**
569 **Zbontar, J., Zitnik, M. and Zupan, B.** (2013) Orange: Data mining toolbox in
570 Python. *J. Machine Learning Res.*, **14**, 2349-2353.
571 **Downie, J.A.** (2014) Legume nodulation. *Curr. Biol.*, **24**, R184-R190.
572 **Durrett, T.P., Gassmann, W. and Rogers, E.E.** (2007) The FRD3-mediated efflux of
573 citrate into the root vasculature is necessary for efficient iron translocation. *Plant*
574 *Physiol.*, **144**, 197-205.
575 **Escudero, V., Abreu, I., Tejada-Jiménez, M., Rosa-Núñez, E., Quintana, J., Isabel**
576 **Prieto, R., Larue, C., Wen, J., Villanova, J., Mysore, K.S., Argüello, J.M.,**
577 **Castillo-Michel, H., Imperial, J. and González-Guerrero, M.** (2019) *Medicago*
578 *truncatula* Ferroportin2 mediates iron import into nodule symbiosomes. *bioRxiv*,
579 630699.
580 **Finney, L.A. and Halloran, T.V.** (2003) Transition metal speciation in the cell: Insights
581 from the chemistry of metal ion receptors. *Science*, **300**, 931.
582 **Flis, P., Ouerdane, L., Grillet, L., Curie, C., Mari, S. and Lobinski, R.** (2016)
583 Inventory of metal complexes circulating in plant fluids: a reliable method based
584 on HPLC coupled with dual elemental and high-resolution molecular mass
585 spectrometric detection. *New Phytol.*, **211**, 1129-1141.
586 **Gage, D.J.** (2002) Analysis of infection thread development using Gfp- and DsRed-
587 expressing *Sinorhizobium meliloti*. *J. Bacteriol.*, **184**, 7042-7046.
588 **Gil-Díez, P., Tejada-Jiménez, M., León-Mediavilla, J., Wen, J., Mysore, K.S.,**
589 **Imperial, J. and González-Guerrero, M.** (2019) MtMOT1.2 is responsible for
590 molybdate supply to *Medicago truncatula* nodules. *Plant Cell Environ.*, **42**, 310-
591 320.
592 **González-Guerrero, M., Matthiadis, A., Sáez, Á. and Long, T.A.** (2014) Fixating on
593 metals: new insights into the role of metals in nodulation and symbiotic nitrogen
594 fixation. *Front. Plant Sci.*, **5**, 45.
595 **González-Guerrero, M., Raimunda, D., Cheng, X. and Argüello, J.M.** (2010) Distinct
596 functional roles of homologous Cu^{+} efflux ATPases in *Pseudomonas aeuginosa*.
597 *Mol. Microbiol.*, **78**, 1246-1258.
598 **González-Guerrero, M., V., E., Sáez, Á. and Tejada-Jiménez, M.** (2016) Transition
599 metal transport in plants and associated endosymbionts. Arbuscular mycorrhizal
600 fungi and rhizobia. *Front. Plant Sci.*, **7**, 1088.
601 **Hakoyama, T., Niimi, K., Yamamoto, T., Isobe, S., Sato, S., Nakamura, Y., Tabata,**
602 **S., Kumagai, H., Umehara, Y., Brossuleit, K., Petersen, T.R., Sandal, N.,**
603 **Stougaard, J., Udvardi, M.K., Tamaoki, M., Kawaguchi, M., Kouchi, H. and**
604 **Suganuma, N.** (2012) The integral membrane protein SEN1 is required for
605 symbiotic nitrogen fixation in *Lotus japonicus* nodules. *Plant Cell Physiol.*, **53**,
606 225-236.
607 **Hakoyama, T., Watanabe, H., Tomita, J., Yamamoto, A., Sato, S., Mori, Y., Kouchi,**
608 **H. and Suganuma, N.** (2009) Nicotianamine synthase specifically expressed in
609 root nodules of *Lotus japonicus*. *Planta*, **230**, 309-317.

bioRxiv preprint doi: https://doi.org/10.1101/717983; this version posted July 29, 2019. The copyright holder for this preprint (which was not certified by peer review) is the author/funder, who has granted bioRxiv a license to display the preprint in perpetuity. It is made available under aCC-BY-NC-ND 4.0 International license.

610 **Hardy, R.W., Holsten, R.D., Jackson, E.K. and Burns, R.C.** (1968) The acetylene-
611 ethylene assay for n(2) fixation: laboratory and field evaluation. *Plant Physiol.*,
612 **43**, 1185-1207.
613 **Haydon, M.J., Kawachi, M., Wirtz, M., Hillmer, S., Hell, R. and Krämer, U.** (2012)
614 Vacuolar nicotianamine has critical and distinct roles under iron deficiency and
615 for zinc sequestration in Arabidopsis. *Plant Cell*, **24**, 724-737.
616 **Higuchi, K., Suzuki, K., Nakanishi, H., Yamaguchi, H., Nishizawa, N.K. and Mori,**
617 **S.** (1999) Cloning of nicotianamine synthase genes, novel genes involved in the
618 biosynthesis of phytosiderophores. *Plant Physiol.*, **119**, 471-480.
619 **Hoffman, B.M., Lukoyanov, D., Yang, Z.Y., Dean, D.R. and Seefeldt, L.C.** (2014)
620 Mechanism of nitrogen fixation by nitrogenase: The next stage. *Chem. Rev.*, **114**,
621 4041-4062.
622 **Inoue, H., Higuchi, K., Takahashi, M., Nakanishi, H., Mori, S. and Nishizawa, N.K.**
623 (2003) Three rice nicotianamine synthase genes, OsNAS1, OsNAS2, and
624 OsNAS3 are expressed in cells involved in long-distance transport of iron and
625 differentially regulated by iron. *Plant J.*, **36**, 366-381.
626 **Inskeep, W.P. and Bloom, P. R.** (1985) Extinction coefficients of chlorophyll a and b
627 in N,N-dimethylformamide and 80% acetone. *Plant Physiol.*, **77**, 483-485.
628 **Jain, A., Wilson, G.T. and Connolly, E.L.** (2014) The diverse roles of FRO family
629 metalloreductases in iron and copper homeostasis. *Front. Plant Sci*, **5**, 100.
630 **Johnson, S.E. and Mohler, C.L.** (2009) *Crop rotation on organic farms: A planning*
631 *manual*: National Resource, Agricultrue and Engineering Services.
632 **Klatte, M., Schuler, M., Wirtz, M., Fink-Straube, C., Hell, R. and Bauer, P.** (2009)
633 The analysis of Arabidopsis nicotianamine synthase mutants reveals functions for
634 nicotianamine in seed iron loading and iron deficiency responses. *Plant Physiol.*,
635 **150**, 257-271.
636 **Kobayashi, T. and Nishizawa, N.K.** (2012) Iron uptake, translocation, and regulation in
637 higher plants. *Annu. Rev. Plant Biol.*, **63**, 131-152.
638 **Kondorosi, E., Mergaert, P. and Kereszt, A.** (2013) A paradigm for endosymbiotic life:
639 Cell differentiation of *Rhizobium* bacteria provoked by host plant factors. *Annu.*
640 *Rev. Microbiol.*, **67**, 611-628.
641 **Kryvoruchko, I.S., Routray, P., Sinharoy, S., Torres-Jerez, I., Tejada-Jiménez, M.,**
642 **Finney, L.A., Nakashima, J., Pislariu, C.I., Benedito, V.A., González-**
643 **Guerrero, M., Roberts, D.M. and Udvardi, M.K.** (2018) An iron-activated
644 citrate transporter, MtMATE67, is required for symbiotic nitrogen fixation. *Plant*
645 *Physiol.*, **176**, 2315-2329.
646 **Kumar, R.K., Chu, H.H., Abundis, C., Vasques, K., Rodriguez, D.C., Chia, J.-C.,**
647 **Huang, R., Vatamaniuk, O.K. and Walker, E.L.** (2017) Iron-nicotianamine
648 transporters are required for proper long distance iron signaling. *Plant Physiol.*,
649 **175**, 1254.
650 **Larue, C., Castilo-Michel, H., Sobanska, S., Cécillon, L., Bureau, S., Barthès, V.,**
651 **Ouerdane, L., Carrière, M. and Sarret, G.** (2014) Foliar exposure of the crop
652 *Lactuca sativa* to silver nanoparticles: evidence for internalization and changes in
653 Ag speciation. *J. Hazard. Mater.*, **264**, 98-106.
654 **León-Mediavilla, J., Senovilla, M., Montiel, J., Gil-Díez, P., Saez, Á., Kryvoruchko,**
655 **I.S., Reguera, M., Udvardi, M.K., Imperial, J. and González-Guerrero, M.**
656 (2018) MtMTP2-facilitated zinc transport into intracellular compartments is
657 essential for nodule development in *Medicago truncatula*. *Front. Plant Sci.*, **9**,
658 990.

bioRxiv preprint doi: https://doi.org/10.1101/717983; this version posted July 29, 2019. The copyright holder for this preprint (which was not certified by peer review) is the author/funder, who has granted bioRxiv a license to display the preprint in perpetuity. It is made available under aCC-BY-NC-ND 4.0 International license.

LeVier, K., Day, D.A. and Guerinot, M.L. (1996) Iron uptake by symbisomes from soybean root nodules. *Plant Physiol.*, **111**, 893-900.

Montiel, J., Arthikala, M.-K., Cárdenas, L. and Quinto, C. (2016) Legume NADPH oxidases have crucial roles at different stages of nodulation. *Int. J. Mol. Sci.*, **17**, 680.

Moreau, S., Meyer, J.M. and Puppo, A. (1995) Uptake of iron by symbiosomes and bacteroids from soybean nodules. *FEBS Lett.*, **361**, 225-228.

Mus, F., Crook, M.B., Garcia, K., Garcia Costas, A., Geddes, B.A., Kouri, E.D., Paramasivan, P., Ryu, M.H., Oldroyd, G.E., Poole, P.S., Udvardi, M.K., Voigt, C.A., Ane, J.M. and Peters, J.W. (2016) Symbiotic nitrogen fixation and challenges to extending it to non-legumes. *Appl. Environ. Microbiol.*, **82**, 3698-3710.

Nakagawa, T., Kurose, T., Hino, T., Tanaka, K., Kawamukai, M., Niwa, Y., Toyooka, K., Matsuoka, K., Jinbo, T. and Kimura, T. (2007) Development of series of gateway binary vectors, pGWBs, for realizing efficient construction of fusion genes for plant transformation. *J. Biosci. Bioeng.*, **104**, 34-41.

O'Hara, G.W. (2001) Nutritional constraints on root nodule bacteria affecting symbiotic nitrogen fixation: a review. *Aust. J. Exp. Agr.*, **41**, 417-433.

Oldroyd, G.E.D. (2013) Speak, friend, and enter: signalling systems that promote beneficial symbiotic associations in plants. *Nat. Rev. Micro.*, **11**, 252-263.

Preisig, O., Zufferey, R., Thony-Meyer, L., Appleby, C. and Hennecke, H. (1996) A high-affinity cbb3-type cytochrome oxidase terminates the symbiosis- specific respiratory chain of *Bradyrhizobium japonicum*. *J. Bacteriol.*, **178**, 1532-1538.

Ravel, B. and Newville, M. (2005) ATHENA, ARTEMIS, HEPHAESTUS: data analysis for X-ray absorption spectroscopy using IFEFFIT. *J. Synchrotron Radiat.*, **12**, 537-541.

Rellán-Álvarez, R., Abadía, J. and Álvarez-Fernández, A. (2008) Formation of metal-nicotianamine complexes as affected by pH, ligand exchange with citrate and metal exchange. A study by electrospray ionization time-of-flight mass spectrometry. *Rapid Commun. Mass Spectrom.*, **22**, 1553-1562.

Rellán-Álvarez, R., Giner-Martínez-Sierra, J., Orduna, J., Orera, I., Rodríguez-Castrillón, J.Á., García-Alonso, J.I., Abadía, J. and Álvarez-Fernández, A. (2010) Identification of a tri-iron(III), tri-citrate complex in the xylem sap of iron-deficient tomato resupplied with iron: New insights into plant iron long-distance transport. *Plant Cell Physiol.*, **51**, 91-102.

Rodríguez-Haas, B., Finney, L., Vogt, S., González-Melendi, P., Imperial, J. and González-Guerrero, M. (2013) Iron distribution through the developmental stages of *Medicago truncatula* nodules. *Metallomics*, **5**, 1247-1253.

Roschzttardtz, H., Séguéla-Arnaud, M., Briat, J.-F., Vert, G. and Curie, C. (2011) The FRD3 citrate effluxer promotes iron nutrition between symplastically disconnected tissues throughout Arabidopsis development. *Plant Cell*, **23**, 2725-2737.

Roth, L.E. and Stacey, G. (1989) Bacterium release into host cells of nitrogen-fixing soybean nodules: The symbiosome membrane comes from three sources. *Eur. J. Cell Biol*, **49**, 13-23.

Roux, B., Rodde, N., Jardinaud, M.-F., Timmers, T., Sauviac, L., Cottret, L., Carrère, S., Sallet, E., Courcelle, E., Moreau, S., Debellé, F., Capela, D., de Carvalho-Niebel, F., Gouzy, J., Bruand, C. and Gamas, P. (2014) An integrated analysis of plant and bacterial gene expression in symbiotic root

bioRxiv preprint doi: https://doi.org/10.1101/717983; this version posted July 29, 2019. The copyright holder for this preprint (which was not certified by peer review) is the author/funder, who has granted bioRxiv a license to display the preprint in perpetuity. It is made available under aCC-BY-NC-ND 4.0 International license.

nodules using laser-capture microdissection coupled to RNA sequencing. *Plant J.*, **77**, 817-837.

Rubio, L.M. and Ludden, P.W. (2005) Maturation of nitrogenase: a biochemical puzzle. *J. Bacteriol.*, **187**, 405-414.

Rubio, M.C., Becana, M., Sato, S., James, E.K., Tabata, S. and Spaink, H.P. (2007) Characterization of genomic clones and expression analysis of the three types of superoxide dismutases during nodule development in *Lotus japonicus*. *Mol. Plant Microbe Interact.*, **20**, 262-275.

Santos, R., Hérouart, D., Puppo, A. and Touati, D. (2000) Critical protective role of bacterial superoxide dismutase in Rhizobium–legume symbiosis. *Molecular Microbiology*, **38**, 750-759.

Schneider, S., Schintlmeister, A., Becana, M., Wagner, M., Woebken, D. and Wienkoop, S. (2019) Sulfate is transported at significant rates through the symbiosome membrane and is crucial for nitrogenase biosynthesis. *Plant Cell Environ.*, **42**, 1180-1189.

Schuler, M., Rellán-Álvarez, R., Fink-Straube, C., Abadía, J. and Bauer, P. (2012) Nicotianamine functions in the phloem-based transport of iron to sink organs, in pollen development and pollen tube growth in Arabidopsis. *Plant Cell*, **24**, 2380-2400.

Senovilla, M., Castro-Rodríguez, R., Abreu, I., Escudero, V., Kryvoruchko, I., Udvardi, M.K., Imperial, J. and González-Guerrero, M. (2018) *Medicago truncatula* Copper Transporter1 (MtCOPT1) delivers copper for symbiotic nitrogen fixation. *New Phytol*, **218**, 696-709.

Singleton, P.W. and van Kessel, C. (1987) Effect of localized nitrogen availability to soybean half-root systems on photosynthate partitioning to roots and nodules. *Plant Physiology*, **83**, 552.

Smil, V. (1999) Nitrogen in crop production: an account of global flows. *Global Biogeochem. Cycles*, **13**, 647-662.

Solé, V.A., Papillon, E., Cotte, M., Walter, P. and Susini, J.A. (2007) A multiplatform code for the analysis of energy-dispersive X-ray fluorescence spectra. *Spectrochim. Acta B*, **62**, 63-68

Streeter, J.G. (1987) Carbohydrate, organic acid, and amino acid composition of bacteroids and cytosol from soybean nodules. *Plant Physiol.*, **85**, 768-773.

Takanashi, K., Yokosho, K., Saeki, K., Sugiyama, A., Sato, S., Tabata, S., Ma, J.F. and Yazaki, K. (2013) LjMATE1: a citrate transporter responsible for iron supply to the nodule infection zone of *Lotus japonicus*. *Plant Cell Physiol.*, **54**, 585-594.

Tang, C., Robson, A.D. and Dilworth, M.J. (1991) Which stage of nodule initiation in *Lupinus angustifolius* L. is sensitive to iron deficiency? *New Phytol.*, **117**, 243-250.

Tejada-Jiménez, M., Castro-Rodríguez, R., Kryvoruchko, I., Lucas, M.M., Udvardi, M., Imperial, J. and González-Guerrero, M. (2015) *Medicago truncatula* Natural Resistance-Associated Macrophage Protein1 is required for iron uptake by rhizobia-infected nodule cells. *Plant Physiol.*, **168**, 258-272.

Tejada-Jiménez, M., Gil-Diez, P., Leon-Mediavilla, J., Wen, J., Mysore, K.S., Imperial, J. and Gonzalez-Guerrero, M. (2017) *Medicago truncatula* molybdate transporter type 1 (MOT1.3) is a plasma membrane molybdenum transporter required for nitrogenase activity in root nodules under molybdenum deficiency. *New Phytol*, **216**, 1223-1235.

bioRxiv preprint doi: https://doi.org/10.1101/717983; this version posted July 29, 2019. The copyright holder for this preprint (which was not certified by peer review) is the author/funder, who has granted bioRxiv a license to display the preprint in perpetuity. It is made available under aCC-BY-NC-ND 4.0 International license.

Terry, R.E., Soerensen, K.U., Jolley, V.D. and Brown, J.C. (1991) The role of active *Bradyrhizobium japonicum* in iron stress response of soy-beans. *Plant Soil*, **130**, 225-230.

Udvardi, M. and Poole, P.S. (2013) Transport and metabolism in legume-rhizobia symbioses. *Annu. Rev. Plant Biol.*, **64**, 781-805.

Valentine, A.J., Kleinert, A. and Benedito, V.A. (2017) Adaptive strategies for nitrogen metabolism in phosphate deficient legume nodules. *Plant Science*, **256**, 46-52.

Vasse, J., de Billy, F., Camut, S. and Truchet, G. (1990) Correlation between ultrastructural differentiation of bacteroids and nitrogen fixation in alfalfa nodules. *J. Bacteriol.*, **172**, 4295-4306.

Vernoud, V., Journet, E.P. and Barker, D.G. (1999) *MtENOD20*, a Nod factor-inducible molecular marker for root cortical cell activation. *Mol. Plant Microbe Interact.*, **12**, 604-614.

von Wiren, N., Klair, S., Bansal, S., Briat, J.-F., Khodr, H., Shioiri, T., Leigh, R.A. and Hider, R.C. (1999) Nicotianamine chelates both FeIII and FeII. Implications for metal transport in plants. *Plant Physiol.*, **119**, 1107-1114.

Waters, B.M., Chu, H.-H., DiDonato, R.J., Roberts, L.A., Eisley, R.B., Lahner, B., Salt, D.E. and Walker, E.L. (2006) Mutations in *Arabidopsis Yellow Stripe-Like1* and *Yellow Stripe-Like3* reveal their roles in metal ion homeostasis and loading of metal ions in seeds. *Plant Physiol.*, **141**, 1446-1458.

Xiao, T.T., Schilderink, S., Moling, S., Deinum, E.E., Kondorosi, E., Franssen, H., Kulikova, O., Niebel, A. and Bisseling, T. (2014) Fate map of *Medicago truncatula* root nodules. *Development*, **141**, 3517-3528.

bioRxiv preprint doi: https://doi.org/10.1101/717983; this version posted July 29, 2019. The copyright holder for this preprint (which was not certified by peer review) is the author/funder, who has granted bioRxiv a license to display the preprint in perpetuity. It is made available under aCC-BY-NC-ND 4.0 International license.

793 **Table 1:** Iron speciation (%) in WT and *nas2-1* nodules. n.d. = not detected.

	WT				*nas2-1*			
Region	Fe(II)-S	Fe(II)-O/N	Fe(III)-O	R^2	Fe(II)-S	Fe(II)-O/N	Fe(III)-O	R^2
ZII	4	12	83	00004	n.d.	14	86	0.0008
IZ	13	19	69	0.0004	5	17	78	0.0006
ZIII	50	24	27	0.001	14	49	37	0.0005
Vessels	n.d.	22	79	0.0008	n.d.	22	78	0.001

794

795

796

797

798

799

800

801

802

803

804

805

806

807

808

809

810

811

812

813

814

815

bioRxiv preprint doi: https://doi.org/10.1101/717983; this version posted July 29, 2019. The copyright holder for this preprint (which was not certified by peer review) is the author/funder, who has granted bioRxiv a license to display the preprint in perpetuity. It is made available under aCC-BY-NC-ND 4.0 International license.

FIGURE LEGENDS

Figure 1. *MtNAS2* is expressed in roots and nodules of *M. truncatula*. (A) Expression data was normalized to the expression of ubiquitin conjugating enzyme E2 gene (*Medtr7g116940*) as standard. Data are the mean ± SE of three independent experiments with 4 pooled plants. (B) *Tnt1* insertion in the only exon of *MtNAS2* causes loss of *MtNAS2* transcripts. Expression was determined in 28 dpi roots and nodules of wild-type (WT) and *nas2-1* plants. Data was relativized to the expression of ubiquitin conjugating enzyme E2 (*Medtr7g116940*) and expressed as mean ± SE of three independent experiments with 4 pooled plants.

Figure 2. *MtNAS2* is required for nitrogen fixation. (A) Growth of representative wild-type (WT), *nas2-1*, and *nas2-1* plants transformed with *MtNAS2* controlled by its own promoter (*nas2-1 MtNAS2*). Bar = 1.5 cm. (B) Fresh weight of WT, *nas2-1*, and *nas2-1 MtNAS2* plants. Data are the mean ± SE of at least 9 transformed plants. (C) Detail of representative nodules of WT, *nas2-1*, and *nas2-1 MtNAS2* plants. Bars = 500 µm. (D) Number of nodules in 28 dpi WT, *nas2-1*, and *nas2-1 MtNAS2* plants. Data are the mean ± SE of at least 9 transformed plants. (E) Nitrogenase activity in 28 dpi nodules from WT, *nas2-1*, and *nas2-1 MtNAS2* plants. Acetylene reduction was measured in duplicate from three sets of three-four pooled plants. Data are the mean ± SE. * indicates statistically significant differences ($p<0.05$).

Figure 3. *MtNAS2* is not required for plant growth under non-symbiotic conditions. (A) Growth of representative wild-type (WT) and *nas2-1* plants when watered with a nutrient solution supplemented with ammonium nitrate and not inoculated with *S. meliloti*. Bar = 1.5 cm. (B) Fresh weight of WT and *nas2-1* plants. Data are the mean ± SE of at least 5 plants. (C) Chlorophyll concentration of wild-type and *nas2-1* plants. Data are the mean ± SE of two sets of 5 pooled plants.

Figure 4. *MtNAS2* is expressed in the root vasculature and in the interzone, zone III, and vessels in nodules. (A) GUS staining of 28 dpi *M. truncatula* roots and nodules expressing the *gus* gene under the control of *MtNAS2* promoter region. Bar = 200 µm. (B) Longitudinal section of a GUS-stained 28 dpi *M. truncatula* nodule expressing the *gus* gene under the control of *MtNAS2* promoter region. ZI indicates Zone I; ZII, Zone II; IZ, Interzone; and ZIII, Zone III. Bar = 200 µm. (C) Cross section of a GUS-stained 28 dpi *M. truncatula* nodule expressing the *gus* gene under the control of *MtNAS2* promoter

bioRxiv preprint doi: https://doi.org/10.1101/717983; this version posted July 29, 2019. The copyright holder for this preprint (which was not certified by peer review) is the author/funder, who has granted bioRxiv a license to display the preprint in perpetuity. It is made available under aCC-BY-NC-ND 4.0 International license.

848 region. Bar = 200 μm. (D) Cross section of a GUS-stained 28 dpi *M. truncatula* root
849 expressing the *gus* gene under the control of *MtNAS2* promoter region. Bar = 50 μm.

850 **Figure 5.** MtNAS2 is located in the nodule core cells, in the endodermis of the nodule
851 vessels, and in cells surrounding the xylem in the root vasculature. (A) Longitudinal
852 section of a 28 dpi *M. truncatula* nodule expressing *MtNAS2-HA* under its own promoter.
853 The three C-terminal HA epitopes were detected using an Alexa594-conjugated antibody
854 (red, left panel). Transformed plants were inoculated with a GFP-expressing *S. meliloti*
855 (green, middle panel). Both images were overlaid with the transillumination image (right
856 panel). ZI indicates Zone I; ZII, Zone II; IZ, Interzone; and ZIII, Zone III. Bars = 100 μm.
857 (B) Detail of the zone III of a 28 dpi *M. truncatula* nodule expressing *MtNAS2-HA* under
858 its own promoter. Left panel corresponds to the Alexa594 signal used to detect the HA-
859 tag, middle panel corresponds to the GFP channel showing *S. meliloti*, and the two were
860 overlaid with the bright field channel in the right panel. Bars = 50 μm (C) Cross section
861 of a nodule vessel from a 28 dpi *M. truncatula* nodule expressing *MtNAS2-HA* under its
862 own promoter. Left panel corresponds to the Alexa594 signal used to detect the HA-tag,
863 middle panel corresponds to the bright field channel showing *S. meliloti*, and the two were
864 overlaid in the right panel. Bars = 50 μm. (D) Cross section from a 28 dpi *M. truncatula*
865 root expressing *MtNAS2-HA* under its own promoter. Left panel corresponds to the
866 Alexa594 signal used to detect the HA-tag, middle panel corresponds to autofluorescence
867 signal of xylem, and the two were overlaid with the bright field channel in the right panel.
868 Bars = 100 μm.

869 **Figure 6.** *MtNAS2* is required for iron distribution and speciation in nodules. (A) Iron
870 (left panel), copper (middle panel), and zinc (right panel) concentration in shoots, roots,
871 and nodules from 28 dpi wild-type (WT) and *nas2-1* plants. Data are the mean ± SE of
872 three sets of three-four pooled organs. (B) Synchrotron-based X-ray fluorescence images
873 of WT (left panels) or *nas2-1* (right panels) showing calcium (top panels) or iron (center
874 panels) distribution in 28 dpi nodules. Lower panels are the overlaid iron and calcium
875 distribution (iron is indicated in red and calcium in green). ZI indicates Zone I; ZII, Zone
876 II; IZ, Interzone; and ZIII, Zone III. Bars = 100 μm. (C) XANES spectra obtained from
877 different regions of WT and *nas2-1* nodules. (D) Decomposition of the Zone III signal
878 into its two principal components.

bioRxiv preprint doi: https://doi.org/10.1101/717983; this version posted July 29, 2019. The copyright holder for this preprint (which was not certified by peer review) is the author/funder, who has granted bioRxiv a license to display the preprint in perpetuity. It is made available under aCC-BY-NC-ND 4.0 International license.

FIGURE 1

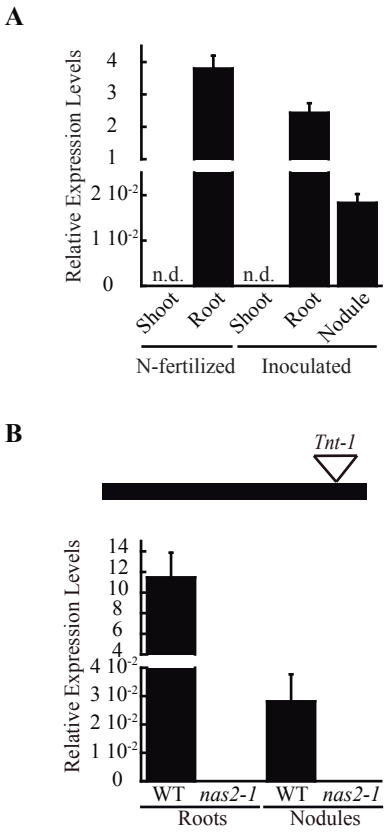

bioRxiv preprint doi: https://doi.org/10.1101/717983; this version posted July 29, 2019. The copyright holder for this preprint (which was not certified by peer review) is the author/funder, who has granted bioRxiv a license to display the preprint in perpetuity. It is made available under aCC-BY-NC-ND 4.0 International license.

FIGURE 2

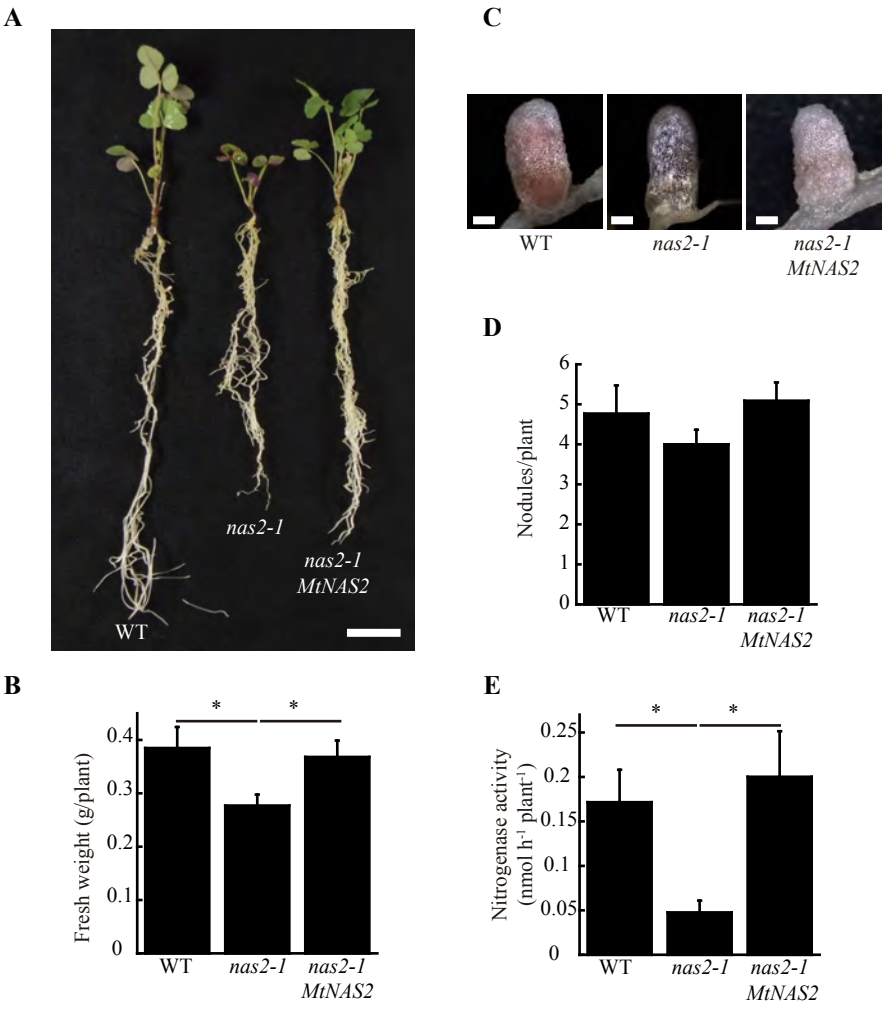

bioRxiv preprint doi: https://doi.org/10.1101/717983; this version posted July 29, 2019. The copyright holder for this preprint (which was not certified by peer review) is the author/funder, who has granted bioRxiv a license to display the preprint in perpetuity. It is made available under aCC-BY-NC-ND 4.0 International license.

FIGURE 3

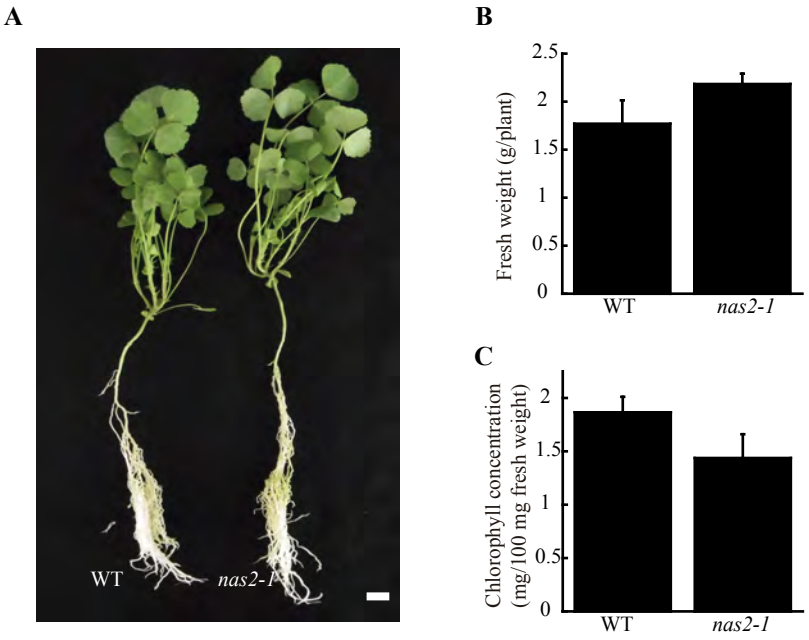

bioRxiv preprint doi: https://doi.org/10.1101/717983; this version posted July 29, 2019. The copyright holder for this preprint (which was not certified by peer review) is the author/funder, who has granted bioRxiv a license to display the preprint in perpetuity. It is made available under aCC-BY-NC-ND 4.0 International license.

FIGURE 4

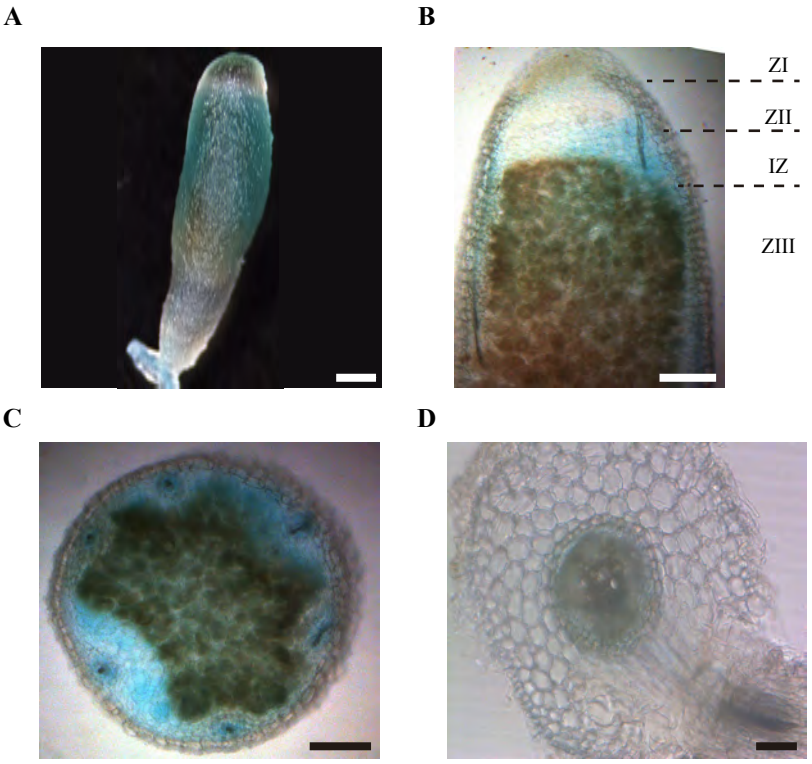

bioRxiv preprint doi: https://doi.org/10.1101/717983; this version posted July 29, 2019. The copyright holder for this preprint (which was not certified by peer review) is the author/funder, who has granted bioRxiv a license to display the preprint in perpetuity. It is made available under aCC-BY-NC-ND 4.0 International license.

FIGURE 5

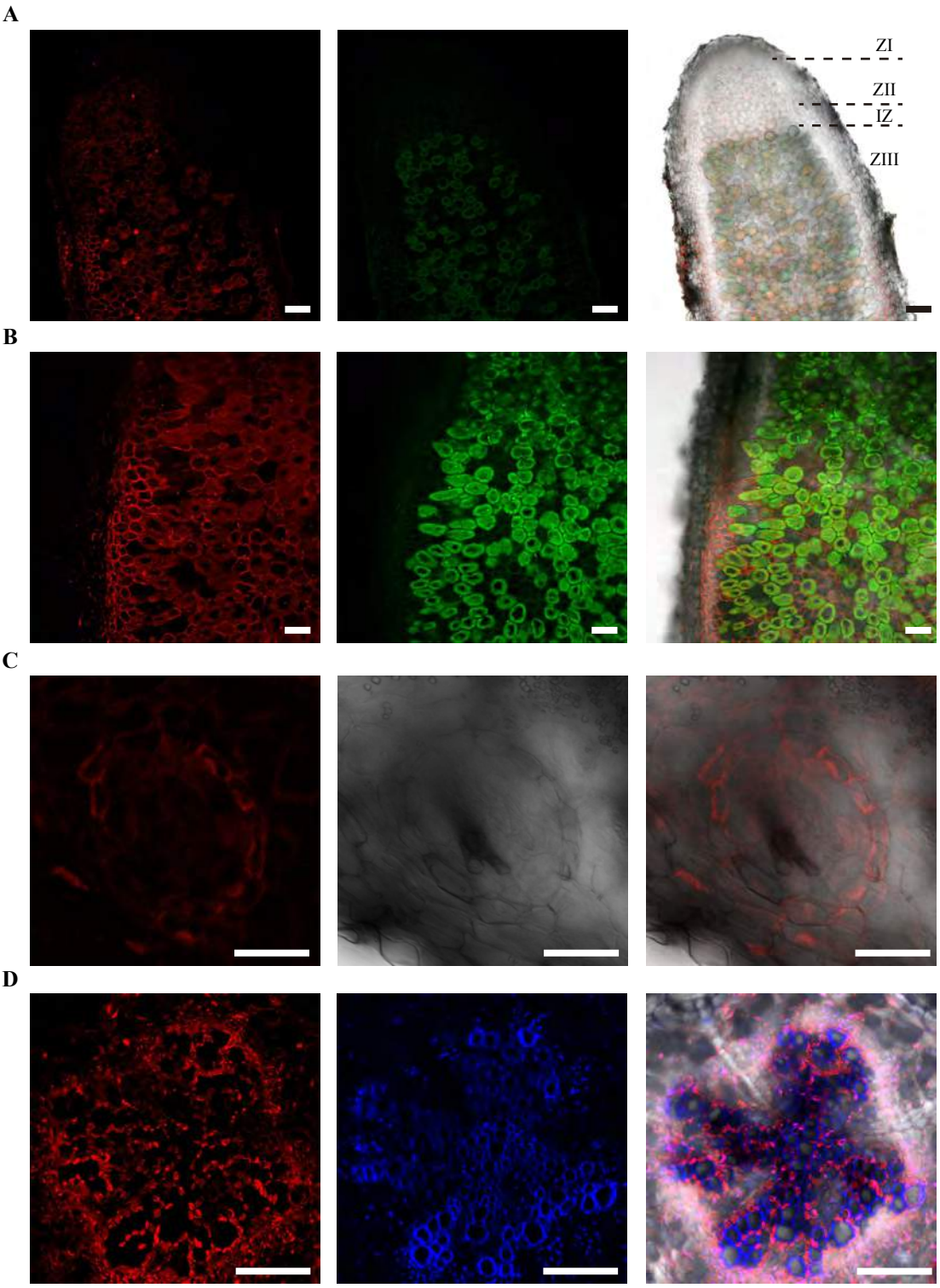

bioRxiv preprint doi: https://doi.org/10.1101/717983; this version posted July 29, 2019. The copyright holder for this preprint (which was not certified by peer review) is the author/funder, who has granted bioRxiv a license to display the preprint in perpetuity. It is made available under aCC-BY-NC-ND 4.0 International license.

FIGURE 6